

# Water Resources Research®

## RESEARCH ARTICLE

10.1029/2023WR036503

# Roughness and Energy Losses Induced by Mussel Growth on the Walls of Hydraulic Structures and Application to a Water Transfer Project



### Key Points:

- The hydraulic roughness of a mussel-attached wall is quantified as a function of the mussel size and mussel attachment density
- A threshold criterion is proposed for the importance of the mussel's filtering activity on the roughness
- An engineering method is proposed and illustrated for quantifying the energy losses induced by heterogeneous patches of mussel on walls

### Supporting Information:

Supporting Information may be found in the online version of this article.

### Correspondence to:

M. Xu,  
mzxu@tsinghua.edu.cn

### Citation:

Zhang, J., Xu, M., Huber, B., Grünzner, M., & Blanckaert, K. (2025). Roughness and energy losses induced by mussel growth on the walls of hydraulic structures and application to a water transfer project. *Water Resources Research*, 61, e2023WR036503. <https://doi.org/10.1029/2023WR036503>

Received 18 OCT 2023

Accepted 9 DEC 2024

Jiahao Zhang<sup>1,2</sup> , Mengzhen Xu<sup>1</sup> , Boris Huber<sup>3</sup>, Markus Grünzner<sup>4</sup>, and Koen Blanckaert<sup>3</sup>

<sup>1</sup>State Key Laboratory of Hydroscience and Engineering, Tsinghua University, Beijing, China, <sup>2</sup>National Inland Waterway Regulation Engineering Research Center, Chongqing Jiaotong University, Chongqing, China, <sup>3</sup>Institute of Hydraulic Engineering and Water Resources Management, Faculty of Civil and Environmental Engineering, TU Wien, Vienna, Austria, <sup>4</sup>Flow Science Deutschland GmbH, Rottenburg, Germany

**Abstract** Mussel biofouling increases energy losses in hydraulic structures. The first contribution of this paper is the quantification of the mussel-induced equivalent sand roughness  $k_s$  as function of the mussel attachment density  $N$  and the shell length  $L$ . Laboratory experiments reveal that  $k_s/L \approx 1.5$  for a continuous regular layer of mussels, which is found for  $N L^2 > 1.2$ . For  $0.5 < N L^2 < 1.2$ , the mussels form a continuous irregular roughness layer with increased values of  $k_s/L$  of up to 2.4. These geometrical irregularities are interpreted as macro-roughness elements, that is, roughness elements with a spatial scale larger than that of an individual mussel. For  $N L^2 < 0.5$ , the density of the irregularities is too low to act as macro-roughness elements leading to  $k_s/L < 1.5$ . The second contribution is the establishment of a threshold criterion for the importance of filtering activity on  $k_s$  based on data from the here reported experiments and data reported in literature in other configurations and/or with other mussel species. It is found that laboratory conditions are often close to the threshold value but that mussel filtering is always negligible in large hydraulic structures. The third contribution is the development of a method based on 3-D numerical simulations for estimating a Darcy-Weisbach friction factor  $f$  for walls that are only partially covered with patches of mussels. An application example illustrates how the thus obtained  $f$  can be used in a 1-D model for quantifying the additional energy losses in large water transfer projects.

**Plain Language Summary** Mussel biofouling is the colonization of walls by mussels. The mussels accumulate at walls in the form of patches that expand. Mussel biofouling increases the wall roughness and hence the frictional energy losses in water transfer projects, such as a grand Water Transfer Project (G-WTP) of China. At present, there are no methods to quantify the biofouling-induced wall roughness and energy losses. Based on laboratory experiments with mussels sampled in a natural river, this paper quantifies the wall roughness as a function of the mussel size and the density of the mussel attachment at the wall. It is found that the mussels considerably increase the wall roughness. Hydrodynamic theory can provide the additional energy losses as a function of the wall roughness for walls with homogeneous mussel patterns, but not for wall with non-homogeneous patchy mussel patterns. For the latter configurations, a method for estimating the additional energy losses is developed based on a 3-D numerical model. Application of this model to the G-WTP shows high biofouling-induced energy losses. The methods for quantifying the biofouling-induced wall roughness and energy losses can be applied to a broad range of hydraulic structures.

## 1. Introduction

Biofouling is the gradual accumulation of waterborne organisms on man-made and natural surfaces submerged in water. Inter-basin water transfer projects, which aim to alleviation of water scarcity, break the biogeographic isolation of watersheds, create invasion highways for species (Zhan et al., 2015) and are also susceptible to biofouling. They provide habitats with abundant food resources and lack of competition for some invasive species, such as mussels. Mussel biofouling causes serious problems to water transfer projects, such as plugging pipes, corroding concrete or metal structures, affecting the safety and operation of mobile structures, and modifying the flow (Lazzarin et al., 2023) and thereby increasing the wall roughness and frictional energy losses (Darrigran, 2002; Ricciardi, 1998; Yao et al., 2017). The focus of the present paper is on the increased wall roughness and frictional energy losses induced by biofouling by golden mussels (*Limnoperna fortunei*, Dunker, 1856). The golden mussel is one of the common biofouling organisms in freshwater. It is native to Asia

© 2025. The Author(s).

This is an open access article under the terms of the [Creative Commons Attribution-NonCommercial-NoDerivs License](#), which permits use and distribution in any medium, provided the original work is properly cited, the use is non-commercial and no modifications or adaptations are made.

and was accidentally introduced to South America in the 1990s. The abilities to tolerate a wide range of environmental conditions (Liu et al., 2020) and to form large colonies make golden mussels particularly challenging to control in water transfer projects (Boltovskoy, 2015).

The question of roughness and energy losses induced by golden mussel biofouling is of interest to a broad audience. The estimation of the additional energy losses and strategies to mitigate them are crucial to engineers and managers dealing with large hydraulic structures. The mechanical processes underlying the additional energy losses and methods to quantify them are important to fluid mechanicians and hydraulic engineers. The biological effects of biofouling and their relevance for mitigation strategies are important for biologists.

The relevance of the reported research is illustrated with the case of the 1,400 km long grand Water Transfer Project (G-WTP) of China, which is representative for large water transfer projects (Figure 1a). Golden mussel biofouling in the G-WTP was first observed in 2017 and continues spreading northwards. The golden mussels have an attachment density  $N$  [ind./m<sup>2</sup>], that is, the number of attached mussels per wall area, that varies along the G-WTP, as summarized in Table 1. Moreover, the mussels do not colonize the entire wall, but rather patches at preferential locations (Figures 1b–1d). Figure 1e illustrates the texture of homogeneous patches of mussels for  $N = 1,000, 3,000, 8,000$  and  $13,000$ , respectively, as observed in a water transfer project in Guangdong, China. Questions of broad relevance for the operation of water transfer projects are how important biofouling-induced additional energy losses are and how they can be quantified. The questions whether or not a layer of mussels in large hydraulic structure, characterized by a low value of  $k_s/R_h$  of O (0.01), induces significant energy losses and how to account for patchiness are not trivial at all. In a culvert of the Dongguan-Shenzhen Water Transfer Project in China, for example, Li (2009) observed that biofouling by golden mussels increased the frictional energy losses by 36%. Similar problems were encountered in the Pearl River Delta Water Resources Allocation Project (Qin, 2021) and an irrigation channel in Lake Kasumigaura (Ito & Takimoto, 2013).

According to Prandtl's hydrodynamic boundary layer theory (Prandtl, 1956), the wall roughness is the most important characteristic of a water-conveying structure, such as an open-channel, aqueduct or, tunnel. The wall roughness, which is typically parameterized with the equivalent sand roughness  $k_s$  [mm] according to Nikuradse (1933), determines the resistance to the flow and hence the frictional energy losses and conveyance capacity (Chen et al., 2020; Sandbach et al., 2012). At present, there is no quantitative prediction method for the mussel-biofouling-induced  $k_s$  on rigid impermeable walls.

Additionally, mussels take water in through their inhalant apertures and expel it through their exhalant siphons during feeding and breathing (Sylvester et al., 2005). Beside the physical roughness of the mussel matrix, this filtering activity may also affect the nearby flow and the energy losses (Lazzarin et al., 2023; Wu et al., 2020), resulting in a modified value of  $k_s$ . An important unresolved question is under what conditions the filtering activity of mussels enhances  $k_s$  and the energy losses. This question is relevant, because the killing of attached mussels, without their mechanical removal, has been adopted as a mitigation measure in the past (Ye et al., 2011). A quantitative criterion that indicates when the filtering becomes relevant would also be useful for the design of laboratory experiments with mussels and for the interpretation of scale effects.

Due to the ease of application, a hydraulic analysis for structures that convey flows with one predominant direction is mostly performed with a one-dimensional (1-D) model, in which all information is averaged over the cross-section of the flow. In 1-D models, the frictional energy losses are parameterized with a friction coefficient, such as the commonly used Darcy-Weisbach coefficient ( $f$  [-]) that will be used in this paper. For walls with a homogeneous roughness distribution, hydrodynamic theory provides  $f$  as a function of Re and  $k_s/R_h$ , where Re is the Reynolds number and  $R_h$  the hydraulic radius (Moody, 1944; Rouse, 1943). Walls affected by mussel biofouling, however, do not represent a homogeneous roughness to the flow, because mussels do not colonize the entire wall at once and first appear in patches (Figures 1b–1d). For walls that are only partially covered with patches of mussels, hydrodynamic theory does not allow estimating  $f$  based on the distribution of  $k_s$ . Water engineers and managers would benefit from a standardized methodology for such configurations.

Based on laboratory experiments and 3-D numerical simulations that cover the range of parameters and configurations encountered in large water transfer projects, the present paper has the following objectives: (a) determining the  $k_s$  of a wall homogeneously attached with mussels as a function of the main characteristics of the mussel matrix; (b) investigating the relevance of the mussels' filtering activity on  $k_s$  and establishing a quantitative criterion for it; (c) developing a methodology for estimating  $f$  for walls with patches of mussels; (d) quantifying

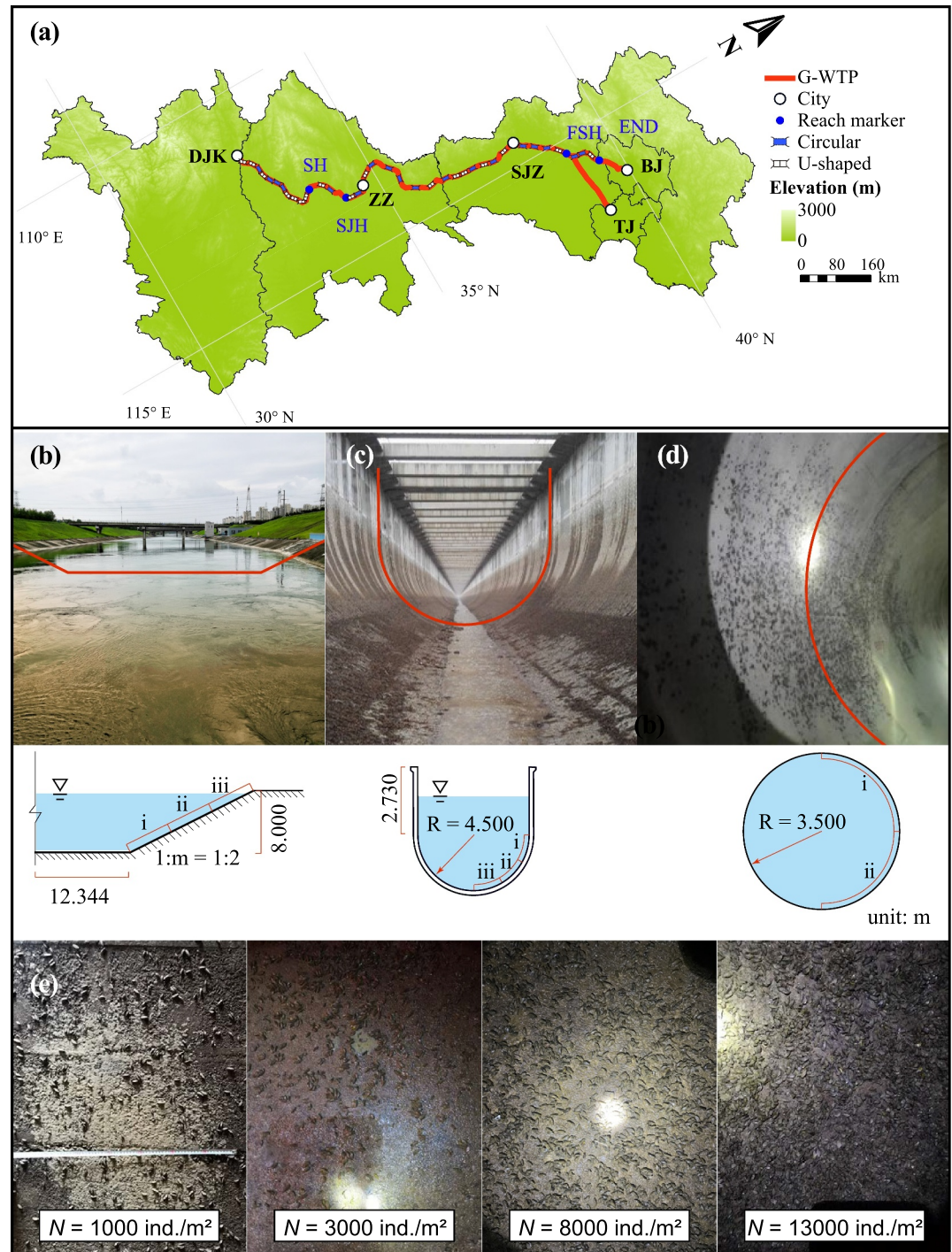


**Figure 1.** Map of the grand Water Transfer Project (G-WTP) with indication of the cross-sectional shapes. ZZ, Zhengzhou; SJZ, Shijiazhuang; TJ, Tianjin; BJ, Beijing. (b) Typical trapezoidal cross-section with open-channel flow; (c) typical U-shaped cross-section with open-channel flow; (d) typical circular cross-section with pressure-driven flow. The numerals in (b)–(d) indicate the patches where golden mussels preferentially attach; they preferentially settle first at (i) and then spread out to locations indicated with higher roman numerals; (e) pictures of patches with mussel densities of  $N = 1,000, 3,000, 8,000$  and  $13,000$  [ind./m<sup>2</sup>].

**Table 1**

Average Mussel Attachment Density  $N$  Observed in Patches of the Wall With Attached Mussels in the Four Reaches of G-WTP (the Observed  $N$  Is Calculated by Our Investigation and Data From Zhao et al., 2019) and Attributed  $k_s$  Value Based on the Results of the Reported Laboratory Investigation

	DJK-SH	SH-SJH	SJH-FSH	FSH-END
Length (km)	249.49	121.87	699.34	125.48
Observed $N$ (ind./m <sup>2</sup> )	1,200	8,100	5,500	100
Attributed $k_s$ (mm)	5	17	27	0

the relevance of mussel biofouling induced additional energy losses and identifying the worst-case configurations in large water transfer projects, by considering the application example of the G-WTP.

## 2. Theoretical Framework

### 2.1. Determining the Equivalent Sand Roughness $k_s$ of a Wall Homogeneously Attached With Mussels

The determination of  $k_s$  is done on the scale of a patch of the wall with homogeneous attachment density  $N$ , that is, the scale is larger than the microtopography of the mussel matrix and the roughness represented by the mussels to the flow can be considered as homogeneous. At this scale,  $k_s$  can be

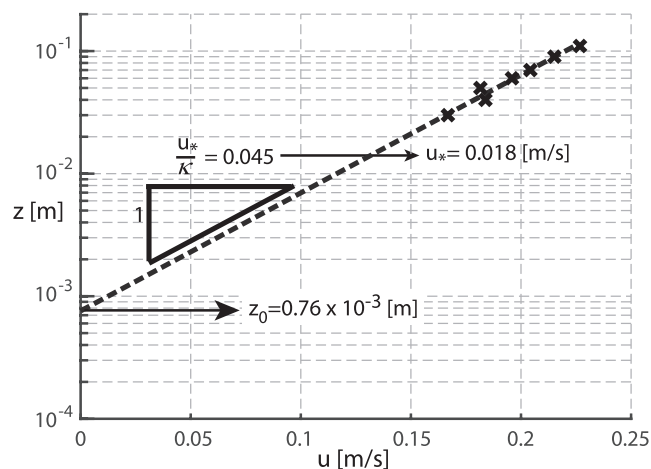
derived from Prandtl's hydrodynamic boundary layer theory, according to which the velocity profile perpendicular to a boundary is logarithmic in a turbulent flow and can be written as (Prandtl, 1956):

$$u(z) = \frac{u_*}{\kappa} \ln\left(\frac{z}{z_0}\right) = \frac{u_*}{\kappa} \ln(z) - \frac{u_*}{\kappa} \ln(z_0) \rightarrow \frac{du}{d(\ln(z))} = \frac{u_*}{\kappa} \quad (1)$$

This velocity profile is valid in the overlapping layer between the inner and outer regions. Here  $u$  is the longitudinal component of the time-averaged velocity,  $u^*$  is the shear velocity,  $\kappa$  is the Karman constant and the  $z$ -axis is perpendicular to the boundary. A constant value of  $\kappa = 0.41$  is appropriate for the investigated configuration of rigid impermeable walls, whereas smaller values of  $\kappa$  have been reported over boundaries that are mobile due to sediment transport (Antico et al., 2019; Ferreira, 2015; Ferreira et al., 2012; Gaudio et al., 2010; Guta et al., 2022, 2024). The reference level  $z_0$  corresponds by definition to the level where  $u = 0$ . The slope of the straight line that fits best to the measured values of  $u$  plotted as a function of  $\ln(z)$  provides an estimate of  $u_*/\kappa$  and the intersection of this best-fitting straight line with the vertical axis provides an estimation of  $z_0$  (Figure 2; Bergeron & Abrahams, 1992).

For the case of a rigid impermeable wall, the value of  $z_0$  generally depends on  $k_s$  and  $\nu/u_*$ , where  $\nu$  is the kinematic viscosity of the water. Nikuradse established on the basis of measurements that  $z_0 = 0.11 \nu/u_*$  in smooth turbulent flow, defined by  $Re_* = u_* k_s / \nu < 5$ , and that  $z_0 = k_s/30$  in rough turbulent flow, defined by  $Re_* > 70$  (Nikuradse, 1932, 1933; Prandtl, 1956). In the intermediate regime of transitional turbulent flow, defined by  $5 < Re_* < 70$ , Rouse (1950, p. 104) and Schlichting and Gersten (2017, p. 531) propose the following analytical relation for roughness elements consisting of a statistical grouping of irregularities of various sizes:

$$z_0 = 0.11 \frac{\nu}{u_*} + \frac{k_s}{30} \quad (2)$$



Hence, the value of  $k_s$  is estimated by (a) fitting a straight line to the measured values of  $u$  plotted as a function of  $\ln(z)$  and deriving the values of  $u_*$  and  $z_0$  as illustrated in Figure 2; (b) computing  $k_s$  by plugging these values of  $u_*$  and  $z_0$  in Equation 2 that relate  $u_*$  and  $z_0$  to  $k_s$  for transitionally and rough turbulent flows, which are the flow regimes in the reported experiments.

The comprehensive literature on the equivalent sand roughness  $k_s$  of gravel beds and different types of biotas provides guidance for relating the thus obtained value of  $k_s$  of a wall homogeneously attached with mussels to the main characteristics of the mussel matrix (objective (i)). Ferreira et al. (2012) and Ferreira (2015) provide a comprehensive review for the case of gravel beds. They highlight that  $k_s$  is not primarily dependent on the grain size distribution of the gravel, but rather on the bed surface complexity. In studies on wall-attached barnacles, Kempf (1937) and Schultz (2007) found that the size of the barnacles and the coverage rate were the main factors that affected  $k_s$ . In an investigation on coral reefs, Carlot et al. (2023) found that  $k_s$  relates to the structural complexity of the coral reef, that is, the number of coral

**Figure 2.** Estimation of  $u_*$  and  $z_0$  from fitting a logarithmic profile to the measured velocities according to Equation 1, illustrated for an experiment with  $Q = 6.52$  l/s and  $N = 5,400$  ind./m<sup>2</sup> (Table 2).

colonies, their width, height and length. In studies on oyster reefs, Styles (2015) found that a good approximation for the physical roughness of oysters is five times the average height of the oysters, while Cannon et al. (2023) found that the surface roughness depends not only on the oyster density and shell length, but also on the structural complexity of the oyster reef canopy. In studies on submerged vegetation, Cheng (2011) and Feng et al. (2024) found that the roughness height is proportional to the vegetation concentration and geometrical characteristics of the vegetation, such as the stem diameter (Cheng, 2011) or the ratio of width to height of the vegetation (Feng et al., 2024).

Based on the guidance of these investigations, we hypothesize that the equivalent sand roughness  $k_s$  of a homogeneous patch of mussels on a rigid impermeable wall depends on the geometrical characteristics of the mussel matrix and on the filtering activity of the mussels. The geometrical characteristics of the mussel matrix can be represented by the mussel shell length  $L$  [m], the attachment density  $N$ , the shape of the mussels as parameterized by their ratio of width:height:length, and the microtopography of the mussel matrix. Hence,  $k_s$  can be generally expressed as:

$$k_s = \text{function}(\text{shell length } L, \text{attachment density } N, \text{width : height : length, microtopography mussel matrix, mussel filtering activity}) \quad (3)$$

When only considering biofouling by golden mussels, the shape of the mussels and the microtopography of the mussel matrix can be assumed as quasi-invariable and it can therefore be expected that  $k_s$  is predominantly related to  $L$  and  $N$ . The equivalent sand roughness  $k_s$  of the mussels can be expected to be proportional to their size as parameterized by the shell length  $L$ , that is,  $k_s \sim L$ . Indeed, increasing the size of the mussels by a factor  $\beta$  for the same mussel shape and structure of the mussel matrix will lead to a corresponding increase of  $k_s$  by a factor  $\beta$ . Obviously, this would lower the attachment density by a factor  $\beta^2$ , that is,  $N \sim L^{-2}$ . Based on these considerations, Equation 3 can be written in nondimensional form as:

$$\frac{k_s}{L} = \text{function}(N L^2, \text{mussel filtering activity}) \quad (4)$$

Objective (i) involves determining the functional relation between  $k_s/L$  and  $N L^2$ , and objective (ii) focuses on investigating the effect of the mussel filtering on this relation.

It should be noted that this theoretical framework is only valid for rigid impermeable walls. Extensions for boundaries that are mobile due to sediment transport or permeable due to hyporheic exchange are reported by Ferreira et al. (2012), Ferreira (2015) and Antico et al. (2019). These authors also report a more detailed dimensional analysis of the parameters affecting the logarithmic velocity profile (Equation 1) and the equivalent sand roughness  $k_s$ .

## 2.2. Estimating the Relevance of the Mussels' Filtering Activity on $k_s$

In a laboratory investigation, Van Duren et al. (2006) found that the importance of the filtering activity of blue mussels, *Mytilus edulis*, depended on the ambient flow conditions: it was significant at low and moderate velocities but limited at high velocities. In another laboratory investigation, Sansom et al. (2018) observed that the filtering activity of fat mucklets, *Lampsilis siliquoidea*, altered the patterns of mean flow and turbulent kinetic energy downstream. The filtering rate of a single golden mussel is in the range from 0.004 to 0.70 [l/ind./hr] (Cataldo et al., 2012; Frau et al., 2013; Pestana et al., 2009; Rückert et al., 2004; Sylvester et al., 2005; Tokumon et al., 2016; Zhang, Xu, & Yang, 2024), with the filtering rate increasing with shell length (Zhang, Xu, & Yang, 2024). The filtering rate of golden mussels is lower than the filtering rate of blue mussels (5.3–7.0 [l/ind./hr] for  $L = 63.5 \pm 6.1$  [mm], Tang and Riisgard (2018)) or fat mucklets (0.14–6.9 [l/ind./hr] for  $L = 9.3 \pm 1.4$  [mm], Sansom et al. (2018)). Golden mussels have, however, a higher attachment density than blue mussels or fat mucklets (Van Duren et al., 2006; Sansom et al., 2020).

In order to establish a quantitative criterion for the relevance of mussel filtering on  $k_s$  (objective (ii)), the ratio of the discharge that is filtered by the mussels to the total discharge,  $Q_{fil}/Q$ , is considered. The discharge filtered by one single mussel,  $Q_{fil,1}$  is typically expressed in units of [l/hr]. The number of mussels contributing to the filtering in one cross-section is equal to  $P N^{1/2}$ , where  $P$  [m] is the part of the wetted perimeter covered with

mussels, and  $N^{1/2}$  [ind./m] is the number of mussels per unit length in the flow direction, under the hypothesis that the mussel matrix is homogeneous. Hence the ratio can be expressed as:

$$\frac{Q_{filt}}{Q} = P N^{\frac{1}{2}} \frac{1}{3.6 \times 10^6} \frac{Q_{filt,1}}{Q} \quad (5)$$

The division by the factor  $3.6 \times 10^{-6}$  accounts for the conversion of  $Q_{filt,1}$  into units of  $[m^3 s^{-1}]$ . This equation reflects that the importance of the filtering activity depends on the filtering capacity of the mussel species,  $Q_{filt,1}$ , and increases with the attachment density. The importance of the filtering activity decreases with increasing discharge, which typically relates to the size of system. A threshold value for the ratio  $Q_{filt}/Q$  will be derived by comparing results from the here reported laboratory and field measurements with golden mussels to the laboratory experiments reported by Van Duren et al. (2006) with blue mussels.

### 2.3. Estimating the Darcy-Weisbach Friction Factor $f$ for Configurations With Mussel Patches

In a 1-D framework that is typically used to investigate large structures that convey flows with one predominant direction, the quantification of the additional energy losses induced by mussel biofouling boils down to the estimation of the Darcy-Weisbach friction factor  $f$ , which is defined as:

$$S_e = f \frac{1}{4R_h} \frac{U^2}{2g} \quad (6)$$

Here  $U$  [m/s] is the cross-sectional averaged velocity. The variable  $S_e$  corresponds to the energy slope in uniform open-channel flow and to the non-dimensional pressure gradient,  $\partial(p/\rho g)/\partial x$  with  $p$  the pressure,  $\rho$  the density of water,  $g$  the gravitational acceleration and  $x$  the distance in flow direction, in pressure-driven flow.

As mentioned in the introduction, hydrodynamic theory allows estimating  $f$  as a function of  $k_s$  for walls that are homogeneously covered with mussels (Moody, 1944; Rouse, 1943), but not for walls that are only partially covered with patches of mussels. Heterogeneous roughness distributions are known to induce 3-D flow pattern, including lateral mass and momentum exchange, cross-channel secondary flow and turbulent vortices (Anderson et al., 2015; Vermaas et al., 2011), which affect the energy losses, but experimental and numerical investigations on heterogeneous roughness distributions remain scarce. Objectives (iii) and (iv) of the present paper are to the importance of heterogeneous patchy roughness distributions and to propose a method that allows estimating the relevance of biofouling-induced additional energy losses in configurations with walls that are partially covered with patches of mussels. The method consists in estimating  $f$  based on 3-D flow simulations, which provide  $U$ ,  $R_h$  and  $S_e$  and allow estimating  $f$  from Equation 6.

The key in the numerical simulations is the appropriate choice of the grid size. It should be larger than the microtopography of the mussel matrix such that the roughness represented by the mussels to the flow can be considered as homogeneous in every grid cell. And it should be small enough such that  $N$  remains constant within the grid cell, that is, it should be significantly smaller than the size of the mussel patch. For an appropriately chosen grid size, the roughness represented to the flow by the mussels is then parameterized by a value of  $k_s$  in every wall-bounded grid cell, which may vary from cell to cell. Technical details of the implementation of the numerical model and its application to the case of the G-WTP are given in the online supporting information.

## 3. Methods

Laboratory experiments with mussels homogeneously attached to the wall were used for objectives (i) and (ii). Because the investigation of mussels organized in patches along the wall was logistically not feasible in the laboratory due to limitations in the size of the experimental flume, 3-D numerical simulations were the key tool with respect to objectives (iii) and (iv). The main link between both is that the 3-D numerical simulations require input on  $k_s$ , as a function of  $N$  and  $L$ , which is provided by the laboratory experiments.

Differences in cross-sectional shape, flow conditions, climatic conditions, mussel attachment density  $N$ , etc., are to be considered in the evaluation of mussel biofouling on  $k_s$  and the energy losses. A parameter range for the laboratory experiments and the 3-D numerical simulations is obtained from the conditions occurring in the G-WTP, which are presented in the next section. The present paper is not a case study on the G-WTP, however,

the G-WTP defines a parameter range that is representative for a broad range of large-scale water transfer projects.

### 3.1. Representative Configurations and Parameter Range Based on the G-WTP

The 1,400 km long G-WTP transfers water from the DJK Reservoir on the Hanjiang River, a 1st order tributary of the Yangtze River that is heavily colonized by golden mussels, northwards to 19 large and medium size cities in the North China Plain, for example, Zhengzhou, Beijing, Tianjin (Figure 1a). The G-WTP consists of 1,131 km with trapezoidal cross-sections with open-channel flow, 21 km of aqueduct with U-shaped cross-sections with open-channel flow and 269 km of circular cross-sections with pressure-driven flow (Figure 1). The cross-sectional geometries are shown in Figures 1b–1d. These three cross-sectional shapes cover the range of geometries found in most water transfer projects. The design discharge  $Q_d$  and maximum discharge  $Q_{max}$  in the upstream reaches are 350 and 420  $\text{m}^3 \text{s}^{-1}$ , respectively. The discharge decreases in downstream direction due to water supply to cities along the pathway of the G-WTP. The design discharge and maximum discharge in the downstream reaches are 265 and 320  $\text{m}^3 \text{s}^{-1}$ , respectively. The discharge in the G-WTP is kept stable, except during maintenance periods, which ensures that the attachment of golden mussels in the G-WTP is not affected by water level variations.

The G-WTP runs through different climatic zones: from a subtropical monsoon climate zone upstream to a temperate monsoon climate zone downstream where water temperature can go below 5°C in winter. The different climatic and hydrodynamic conditions lead to variations in  $N$  along the G-WTP. Consequently, the G-WTP is divided in four reaches (Figure 1a) according to the average  $N$  in patches of the wall with attached mussels, as observed by Zhao et al. (2019) and summarized in Table 1. Note that patches with homogeneous mussel attachment density are defined at the wall, and the patch area is enclosed by the line that connects the outmost mussels of the patch. There is low attachment density in the DJK-SH reach ( $N = 1,200$ ), medium attachment density in the SH-SJH reach ( $N = 5,500$ ), high attachment density in the SJH-FSH reach ( $N = 8,100$ ), and hardly any biofouling in the FSH-END reach ( $N = 100$ ).

The colonization succession of the golden mussels was investigated in situ by Cao et al. (2014) and Zhao et al. (2019). Golden mussels do not colonize the entire wall at once, but spread out from initial preferential locations. In trapezoidal open-channel sections,  $N$  is highest near the toe of the bank and decreases higher on the bank, while it is low on the bottom. In U-shaped sections,  $N$  is high on the semicircles and the connection between the semicircle and side wall, and decreases toward the bottom, and it is low on the vertical walls. In the pressure tunnel sections,  $N$  is high on the top half, while low on the bottom half. The preferential locations for mussel attachment are schematically indicated in Figures 1b–1d: mussel preferentially attached in the locations indicated by the numeral (i) and subsequently spread out in the order of increasing numerals. Non-numbered parts of the cross-section are characterized by low mussel attachment densities.

### 3.2. Laboratory Experiments

Laboratory experiments with live mussels were performed at Tsinghua University in strict adherence to Tsinghua University's general laboratory standards for the ethical treatment of experimental animals.

In order to determine the  $k_s$  of a wall homogeneously attached with mussels, it is important to investigate mussels that are organized in a “natural” porous matrix structure, that is, mussels that have attached at a wall in a natural way instead of artificial mussel arrangements. Therefore, golden mussel colonies attached on bamboos were sampled from the Xizhijiang River, a 2nd order tributary of the Pearl River in South China, and cultivated in the laboratory for the subsequent flume experiments. Two colonized bamboo samples were taken. The shell length in the first and second samples were  $L = 10.8 \pm 1.4$  mm and  $L = 12.3 \pm 2.8$  mm, respectively. These shell lengths are representative for one-year-old golden mussels. Due to the difficulty of overwintering, 1-year old mussels are often the dominant age category in water transfer projects.

The roughness characteristics of the attached mussels were then investigated in a 4 m long PVC flume, with a semi-circular cross-section and a diameter of 0.3 m (Figure 3). The colonized bamboos were installed in the flume in an area of  $1.5 \times 0.2 \text{ m}^2$  with a leading edge (LE in Figure 3) 1.5 m away from the flume inlet. Water imported from the Xizhijiang River was used in the flume in order to guarantee a natural environment for the mussels with water that provides oxygen and food.

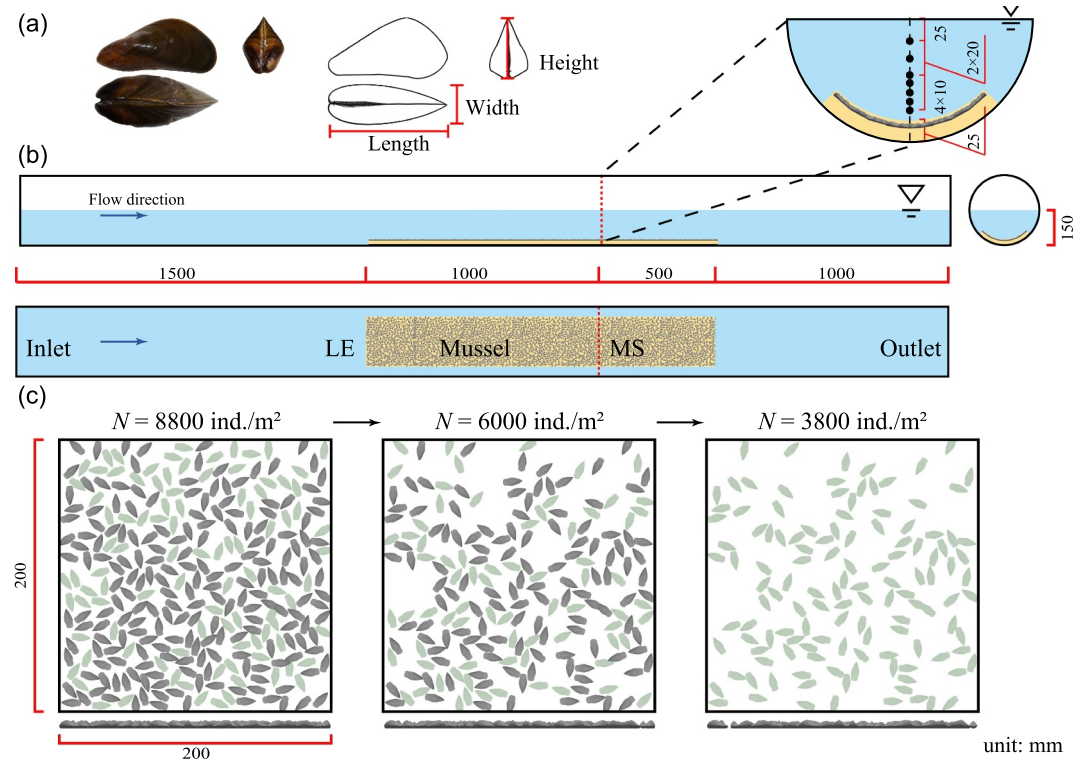


**Figure 3.** Schematic view of the experimental laboratory setup, unit: mm. The bamboo patch including the attached mussels is indicated in yellow, MS indicates the measurement cross-section and LE the leading edge of the bamboo patch. (a) Definition of the mussel length, width and height; (b) side view and top view of the laboratory flume and measurement cross-section with the seven points in the vertical at the channel axis where velocities were measured; (c) schematic illustration of the method for reducing  $N$  while maintaining a staggered arrangement without directional preference. The method is illustrated on scale for the experiments with the second samples of mussels with  $N$  values of 8,800, 6,000 and 3,800 (Table 2); each symbol schematically represents a mussel and dark gray colored symbols represent mussels that were removed while reducing  $N$ .

Obviously, the ratio of the size of the mussels to the size of the flow, as represented by  $L/R_h$ , is at least one order of magnitude smaller in a laboratory flume than in a large hydraulic structure. For dead mussels, Equation 4 indicates that the dependence of  $k_s/L$  on  $N L^2$  primarily depends on the geometric characteristic of the mussel matrix and not primarily on the flow. This statement is valid as long as the flow in the laboratory flume remains fully turbulent and the mussels remain fully submerged. As a consequence, the dependence of  $k_s/L$  on  $N L^2$  for dead mussels as derived from the laboratory experiment can be generalized and remains valid for large hydraulic structures. For alive mussels, Equation 5 indicates that the effect of the filtering depends on the size of the flow and that the effect of the filtering is much larger in small laboratory flumes than in large hydraulic structures. For configurations where the filtering activity does affect the dependence of  $k_s/L$  on  $N L^2$  in the laboratory experiment, the resulting value of  $k_s/L$  cannot be generalized.

Experiments were first done for the highest  $N$  with the mussels attached in a thick continuous layer. The attachment density  $N$  was then reduced in several steps. Mussels were removed by manually cutting off their byssal threads. Mussels were removed in such a way that their arrangement remained staggered and homogeneous without directional preference, that is, they still represent a wall homogeneously attached with mussels. This method of reducing  $N$  is schematically illustrated in Figure 3c for the experiments with the second samples of mussels with  $N$  values of 8,800, 6,000 and 3,800 (Table 2). The investigated attachment densities  $N$  and the experimental conditions are indicated in Table 2.

A first series of experiments was performed with alive mussels from the first sample with  $L = 10.8 \pm 1.4$  mm. The series started with the highest attachment density  $N = 12,000$  [ind./m<sup>2</sup>], and subsequently lower values of  $N = 8,200$ , 5,400 and 3,600 [ind./m<sup>2</sup>] were investigated. At the end of the series, the mussels were inactivated and the experiment with the lowest attachment density of  $N = 3,600$  [ind./m<sup>2</sup>] was repeated with dead mussels. The

**Table 2**  
*Experimental Conditions*

$Q$ [l/s]	Re [-]	$N$ [ind./m <sup>2</sup> ]	State	Shell length $L$ [mm]	$N L^2$ [-]	Number of repetitions		
2.65	6,700	12,000	Alive	10.8 ± 1.4 mm	1.40	3		
		8,200	Alive	10.8 ± 1.4 mm	0.96	3		
		5,400	Alive	10.8 ± 1.4 mm	0.63	3		
		3,600	Alive	10.8 ± 1.4 mm	0.42	3		
		3,600	Dead	10.8 ± 1.4 mm	0.42	3		
		0	/	/	0	3		
		8,800	Alive	12.3 ± 2.8 mm	1.33	3		
		8,800	Dead	12.3 ± 2.8 mm	1.33	3		
		6,000	Dead	12.3 ± 2.8 mm	0.91	3		
		3,800	Dead	12.3 ± 2/8 mm	0.57	3		
		0	/	/	0	3		
		6.52	14,850	12,000	Alive	10.8 ± 1.4 mm	1.40	3
				8,200	Alive	10.8 ± 1.4 mm	0.96	3
5,400	Alive			10.8 ± 1.4 mm	0.63	3		
3,600	Alive			10.8 ± 1.4 mm	0.42	3		
3,600	Dead			10.8 ± 1.4 mm	0.42	3		
0	/			/	0	3		
8,800	Alive			12.3 ± 2.8 mm	1.33	3		
8,800	Dead			12.3 ± 2.8 mm	1.33	3		
6,000	Dead			12.3 ± 2.8 mm	0.91	3		
3,800	Dead			12.3 ± 2/8 mm	0.57	3		
0	/			/	0	3		

*Note.* Discharge  $Q$ ; Reynolds number  $Re = U R_h/\nu$ , with  $U$  the depth-averaged velocity in the measured profile,  $R_h$  the hydraulic radius and  $\nu$  the kinematic viscosity; attachment density  $N$ , and shell length  $L$ .

second series of experiments was performed with mussels from the second sample with  $L = 12.3 \pm 2.8$  mm. First, alive mussels were investigated at the highest attachment density  $N = 8,800$  [ind./m<sup>2</sup>]. Then the mussels were inactivated and experiments were done with dead mussels for decreasing  $N$  values of 8,800, 6,000, 3,800 and 3800 [ind./m<sup>2</sup>]. Comparison of the  $k_s$  values in experiments with alive and dead mussels under similar hydraulic conditions allowed assessing the relevance of the filtering (objective (ii)).

Each mussel configuration ( $N$  and living status) was investigated for two discharges,  $Q = 2.65$  l s<sup>-1</sup> (Reynolds number  $Re = U R_h/\nu = 6,700$ , with  $U$  the depth-averaged velocity in the measured profile,  $R_h$  the hydraulic radius and  $\nu$  the kinematic viscosity) and  $Q = 6.52$  l s<sup>-1</sup> ( $Re = 14,850$ ), and was repeated three times, resulting in six experimental estimations of  $k_s$ . A total number of 66 experiments was performed: 30 with alive mussels, 24 with dead mussels, and 12 without mussels.

In order to estimate  $k_s$  from hydrodynamic theory according to Equations 1 and 2, a velocity profile was measured for each experiment at the axis of the flume in the cross-section (MS in Figure 3) situated 1 m downstream of the bamboo's leading edge with a side-looking Nortek Vectrino Acoustic Doppler Velocimeter (ADV). The quasi-cylindrical measuring volume is located 5 cm from central emitter and has a diameter of 6 mm. The main contribution to the velocity measurement comes from the emitter axis, however, because the intensity of the acoustic field is maximum at the emitter axis and decreases in a Gaussian way with distance perpendicular to the axis, whereby the diameter of the measuring volume is typically defined by a 6 dB decay in acoustic intensity (Hurth & Lemmin, 1998). These characteristics in combination with an elevation difference between the measuring points of 10 mm ensure that the velocity profile is well resolved. It was verified a posteriori by means of 3-D numerical simulations that the flow was fully developed at this location (not shown). Velocity was measured at a frequency of 200 Hz in seven points at the elevations shown in Figure 3 for a period of 30 s. It was

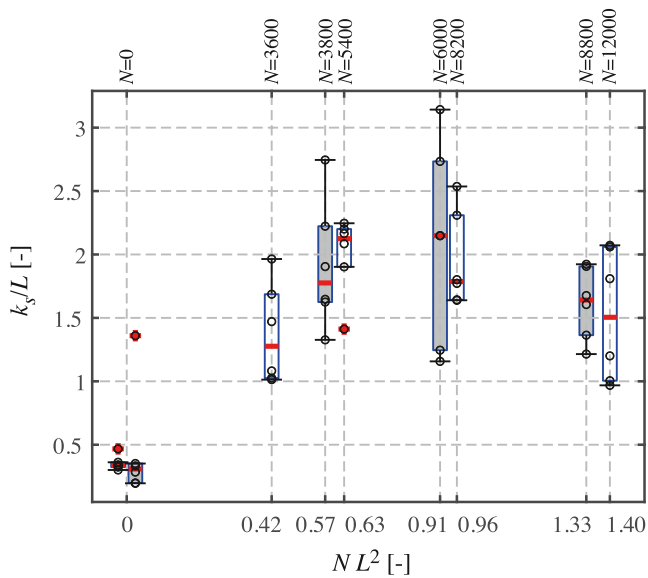


**Figure 4.** Normalized equivalent sand roughness  $k_s/L$  as a function of the normalized mussel attachment density  $N L^2$  for the first series of experiments with alive mussels of  $L = 10.8 \pm 1.4$  mm (empty boxplots) and the second series of laboratory experiments with dead mussels of  $L = 12.3 \pm 2.8$  mm (shaded boxplots). The corresponding values of  $N$  [ind./m<sup>2</sup>] for each experiment are also indicated. For each value of  $N L^2$ , the boxplots indicate the results of 3 repeated experiments for two discharges (cf. Table 2); the circles indicate estimates for the individual experiments. On each box, the central mark indicates the median, and the bottom and top edges of the box indicate the 25th and 75th percentiles  $q_{25}$  and  $q_{75}$ , respectively. The whiskers extend to the most extreme data points not considering outliers. Outliers, defined as data points greater than  $q_{75} + 1.5(q_{75} - q_{25})$  or less than  $q_{25} - 1.5(q_{75} - q_{25})$  (Krzywinski & Altman, 2014), are plotted individually using the '+' symbol. The dashed line represents the trend.

vertical axis) are related, an uncertainty of the order of 30% can also be expected in the estimations of  $z_0$  and  $k_s$ , which complies with the scatter found in the experimental data shown in Figure 4. The six independent estimates for every value of  $N$  allowed for a more accurate estimation of the median value of  $k_s/L$  that clearly reveals the trend of  $k_s/L$  as a function of  $N L^2$ , and which confirms the hypothesis that  $k_s/L$  primarily depends on  $N L^2$  (Equation 4).

The  $k_s/L$  values increase with increasing attachment density onto a maximum value of  $k_s/L \approx 2.2$  in the range of values of  $N L^2 \approx 0.6$  to  $0.9$ . The  $k_s$  values then decrease for larger  $N L^2$  values. A value of  $k_s/L \approx 1.5$  was found for the largest investigated  $N L^2 = 1.4$ . This trend is highlighted with the dashed line in Figure 4.

For  $N L^2 = 1.4$ , the mussels form a continuous regular roughness layer of mussels. The value of  $k_s/L \approx 1.5$  confirms that the equivalent sand roughness  $k_s$  is proportional to a characteristic geometric scale of the mussels, which is a result in line with classical hydrodynamic theory (Dittrich, 1998, p. 29; Hinze, 1975; Nezu & Nakagawa, 1993). Values of  $N L^2 \gg 1.4$  do occur in hydraulic structures. For such values, it is expected that the thickness of the continuous regular layer of mussels increases, without significantly changing its surface texture and  $k_s/L$  value. For values of  $N L^2$  smaller than approximately 1.2, the mussels rather form a continuous irregular roughness layer. For  $N L^2$  larger than approximately 0.5, these geometrical irregularities lead to  $k_s/L$  values higher than that of a continuous regular layer of mussels. These geometrical irregularities are interpreted as macro-roughness elements, that is, roughness elements with a spatial scale larger than that of an individual mussel. These macro-roughness elements can be represented by a  $k_s$  value when modeling the flow on a grid size that is larger than the scale of the macro-roughness elements, as is the case in the present investigation. This is reminiscent of the different roughness scales discussed by Canovaro et al. (2007) and Bertin et al. (2017). For values of  $N L^2$  smaller than approximately 0.5, the density of the irregularities is too low to act as macro-roughness

verified that this measurement period of 30 s was sufficient to obtain stationary statistics on the mean velocity (see online supporting information, Figure S1 in Supporting Information S1), which is the only flow variable of interest in the present paper. The data were de-noised and de-spiked according to the procedure of Goring and Nikora (2002).

## 4. Results and Discussion

### 4.1. Equivalent Sand Roughness $k_s$ as Function of Attachment Density $N$ and Shell Length $L$

Figure 2 illustrates that the measured profiles at the centerline are well approximated by the logarithmic velocity profile of Equation 1. This suggests that the velocity profile at the centerline is mainly affected by the roughness of the mussels installed in the central 0.2 m of the flume and not by the smooth-wall shallower cross-sectional areas at the left and right of the mussels.

Figure 4 shows the  $k_s/L$  values as a function of  $N L^2$ , as estimated from the laboratory experiments for the first series of experiments with alive mussels of  $L = 10.8 \pm 1.4$  mm (empty boxplots) and the second series of experiments with dead mussels of  $L = 12.3 \pm 2.8$  mm (shaded boxplots). The figures are shown in form of boxplots, which are appropriate for sample sizes larger than 5 (Krzywinski & Altman, 2014).

Figure 4 shows that the variance in the estimates of  $k_s/L$  is quite large. Out of the 66 experimental estimations of  $k_s/L$ , 7 estimations deviate by more than 33% from the median value and one of these estimations deviates by more than 55%. According to Equation 2, the uncertainty in the estimation of  $k_s$  is directly related to the uncertainty in the estimations of  $u_*$  and  $z_0$ , both of which are estimated by fitting the logarithmic velocity profile (Equation 1) to the measured data as illustrated in Figure 2. According to Nezu and Nakagawa (1993), the uncertainty in the estimation of  $u_*$  is of the order of 30%. Because the estimations of  $u_*$  (slope in Figure 2) and  $z_0$  (intersect with the

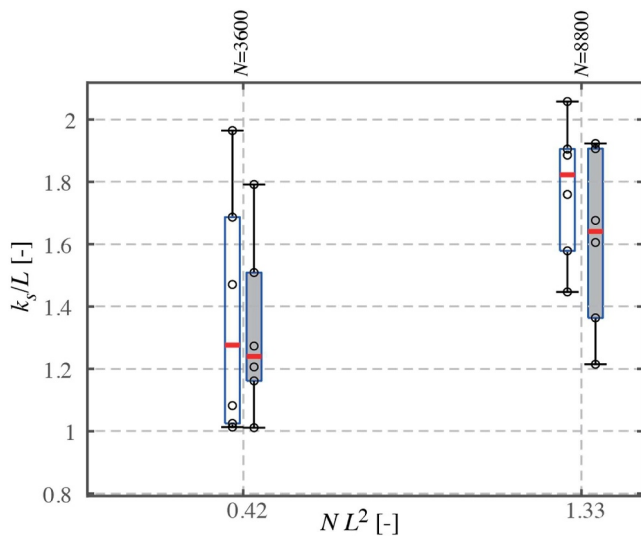


**Figure 5.** Comparison of the normalized equivalent sand roughness  $k_s/L$  of alive (empty boxplots) and dead (shaded boxplots) mussels for the experiment with  $N = 3,600$  [ind./m<sup>2</sup>] and  $L = 10.8 \pm 1.4$  [mm], and the experiment with  $N = 8,800$  [ind./m<sup>2</sup>] and  $L = 12.3 \pm 2.8$  mm. Symbols are further explained in the caption of Figure 4.

elements and the resulting  $k_s/L$  value is smaller than that of a continuous regular layer of mussels. In the investigated range of  $0.42 < N L^2 < 1.40$ , the median values of  $k_s/L$  roughly vary between 1.2 and 2.4. The experimental results suggest that  $k_s/L = 1.5$  is a good approximation for the roughness of a continuous regular layer of mussels, and that  $k_s/L = 2.4$  is a conservative estimation for mussels organized in a continuous irregular layer.

Golden mussels have an elongated, oval shape, and a ratio of width: height: length of 1:1.18:2.60 (Morton, 1973). Some other mussels have a similar shape: zebra mussels, for example, have a ratio of width:height:length of 1:1.06:2.03 (Thomas & Schloesser, 2013), quagga mussels of 1:1.37:2.31 (Thomas & Schloesser, 2013) and blue mussels of 1:1.31:2.35 (Alunno-Bruscia et al., 2001). Because these ratios of width:height:length for different mussel species are quite similar, it can be assumed that the shape of the mussels as represented by the ratio of width:height:length does not exert a dominant control on  $k_s$  (Equation 3) and that the values of  $k_s/L$  as a function of  $N L^2$  found for golden mussels remain good approximations for other mussel species and mussels with different sizes, but similar shapes. These assumptions are further underpinned by the similar roughness length scales and similar non-linear variations in bed roughness as a function of mussel density that were observed for mussel-covered alluvial river beds by Sansom et al. (2020) in laboratory experiments and Sansom et al. (2022) in natural rivers.

#### 4.2. Equivalent Sand Roughness $k_s$ of Alive Versus Dead Mussels and Quantitative Criterion for the Relevance of Mussels' Filtering Activity

Figure 4 suggests that no significant difference exists between the  $k_s$  values of alive and dead mussels. This is further substantiated in Figure 5 where alive and dead mussels are compared for the same mussel matrix in two experiments with identical hydraulic conditions (cf. Table 2). This indicates that the filtering activity does not significantly modify the hydrodynamics in the vicinity of the investigated mussels and that the mussel-induced roughness is essentially due to the geometry of the mussel matrix. Alive mussels are open when actively filtering, whereas dead mussels are closed. This leads to small geometric differences in the mussel matrix that may tentatively explain the slightly higher values of  $k_s$  for the alive mussels. Differences in  $k_s$  between alive and dead mussels are smaller than the uncertainty in the estimation of  $k_s$ , however, and it can be concluded from Figures 4 and 5 that no significant difference exist in the  $k_s$  values of alive and dead mussels in the reported experiments. Further insight in the geometric differences in frontal area between alive and dead mussels and in the combined effect of these geometric differences with the hydrodynamic differences due to the filtering would be valuable to restoration and eco-hydraulic science.

In order to establish a quantitative criterion for the relevance of mussel filtering on  $k_s$ , Table 3 summarizes values of  $Q_{fil}/Q$  estimated from Equation 5 for the laboratory experiments of Van Duren et al. (2006) with blue mussels, the here reported laboratory experiments with golden mussels, and the G-WTP with golden mussels. For the blue mussels, the maximum value of  $Q_{fil,1} = 7.0$  [l/ind./hr] is used in the estimation. For the here reported laboratory

**Table 3**

Estimation of the Ratio of the Discharge That Is Filtered by the Mussels to the Conveyance Discharge,  $Q_{fil}/Q$

	$Q_{fil,1}$ [l/ind./hr]	$N$ [ind./m <sup>2</sup> ]	$Q$ [m <sup>3</sup> /s]	$P$ [m]	$Q_{fil}/Q$ [-]	Effect of mussel filtering on energy losses
Laboratory experiments of Van Duren et al. (2006)	7.0	1,800	0.013	0.6	$3.7 \times 10^{-3}$	Yes
			0.031		$1.6 \times 10^{-3}$	Yes
			0.084		$0.6 \times 10^{-3}$	No
Here reported laboratory experiments	0.35	12,000	$2.65 \times 10^{-3}$	0.2	$0.8 \times 10^{-3}$	No
			$6.52 \times 10^{-3}$		$0.3 \times 10^{-3}$	No
G-WTP	0.70	10,000	350	15	$0.8 \times 10^{-6}$	

experiments, the estimation is done for the highest value of  $N = 12,000$  [ind./m<sup>2</sup>] and the maximum value of  $Q_{\text{filtr},1} = 0.35$  [l/ind./hr] for golden mussels with lengths  $L$  of about 10 mm as found in our laboratory experiments (Zhang, Xu, & Yang, 2024). For the G-WTP, the highest value of  $Q_{\text{filtr},1} = 0.70$  [l/ind./hr] (Cataldo et al., 2012; Frau et al., 2013; Pestana et al., 2009; Rückert et al., 2004; Sylvester et al., 2005; Tokumon et al., 2016; Zhang, Xu, & Yang, 2024) and the maximum observed value of  $N = 8,100$  [ind./m<sup>2</sup>] are taken. These choices yield the highest values of  $Q_{\text{filtr}}/Q$ .

According to the data in Table 3, filtering by blue mussels is relevant in the experiments by Van Duren et al. (2006) when  $Q_{\text{filtr}}/Q > 1.6 \times 10^{-3}$  and negligible when  $Q_{\text{filtr}}/Q < 0.6 \times 10^{-3}$  and filtering by golden mussels is found to be negligible in the here reported experiments when  $Q_{\text{filtr}}/Q < 0.8 \times 10^{-3}$ . The coherence between these values suggests that Equation 5 may be a useful criterion for assessing the relevance of filtering for different mussel species. The data in Table 3 further suggest a threshold value of  $Q_{\text{filtr}}/Q \sim 1 \times 10^{-3}$ . Equation 5 and the data in Table 3 further suggest that the mussels' filtering activity may be relevant in small configurations with small  $Q$ , but is negligible in large configurations such as water-conveying structures with large  $Q$ . Equation 5 and the threshold value provide insight in scale effects and may be helpful in designing and interpreting laboratory experiments. Further experiments with values of  $Q_{\text{filtr}}/Q$  near the assumed threshold value of  $1 \times 10^{-3}$  and with different mussel species would be useful to confirm that Equation 5 is a useful criterion for assessing the relevance of filtering for different mussel species and to confirm the generality of the threshold value.

### 4.3. Application Example

The application to the G-WTP is intended as an example for the modeling of other water transfer projects. The analysis of the mussel-induced energy losses in water transfer projects based on the novel parameterization of  $k_s$  and the method for estimating  $f$  proposed in the present paper consists of the following steps. (a) Definition of the mussel shell length  $L$  and representative values of the attachment density  $N$ , and estimation of  $k_s$  based on Figure 4; (b) definition of a representative cross-sectional geometry and a design discharge and establishment of a 3-D numerical model; (c) definition of the patchiness of the mussel biofouling and attribution of the appropriate  $k_s$  value in every grid cell; (d) estimation of the Darcy-Weisbach friction coefficient  $f$  from the numerical data according to Equation 6 and analysis of the results. As an application example, the relevance of the energy losses induced by mussel biofouling in the G-WTP are quantitatively estimated and the worst-case scenario in terms of patchiness of the mussels and attachment density  $N$  is identified hereafter (objective (iv)).

- i. definition of the mussel shell length  $L$  and representative values of the attachment density  $N$ , and estimation of  $k_s$  based on Figure 4

The shell lengths in the reported laboratory experiments are representative for one-year-old golden mussels, which are the dominant age category in the G-WTP due to the difficulty in overwintering. For the application example, the average mussel length of the laboratory experiments of  $L = 11.55$  mm was adopted.

It is interesting to note that the observed value of  $N = 5,500$  in the longest reach of the G-WTP from SJH to FSH (Figures 1a and Table 1) is in the range that leads to the highest values of  $k_s/L$  of up to 2.4 and the highest additional energy losses. Depending on the size of the mussels, the higher observed value of  $N = 8,100$  in the reach from SH to SJH (Figures 1a and Table 1) can represent a continuous regular layer of mussels with  $k_s/L \sim 1.5$  or a continuous irregular layer with  $1.5 < k_s/L < 2.4$ . No experimental data are available for the value of  $N = 1,200$  observed in the DJK-SH reach, but it can reasonably be assumed that this value is representative of a rather loose mussel layer arrangement that leads to a smaller value of  $k_s/L$ .

Based on these observations and interpretations,  $k_s/L$  values of 0, 0.4, 1.5 and 2.4 have been attributed to the FSH-END reach, the DJK-SH reach, the SJH-FSH reach, and the SH-SJH reach of the G-WTP, respectively. For the case without mussel biofouling ( $k_s/L = 0$ ), the design value of  $k_s = 0.91$  mm of the G-WTP has been adopted. For the cases with biofouling, the corresponding  $k_s$  values are 5 mm, 17 and 27 mm, respectively (Table 1).

- ii. definition of a representative cross-sectional geometry and a design discharge and establishment of a 3-D numerical model

The 3-D numerical model was set-up for the three characteristic cross-sectional geometries (Figures 1b–1d) of the G-WTP. Numerical simulations were performed for the design discharge  $Q_d$  along the G-WTP. The aqueduct reaches consist of three parallel open U-shaped cross-sections (Figure 1c), each having  $Q_d = 350/3 = 116.7$  m<sup>3</sup> s<sup>-1</sup>. The reach with trapezoidal cross-section (Figure 1b) has  $Q_d = 330$  m<sup>3</sup> s<sup>-1</sup> and the pressure-tunnel (Figure 1d) reaches consists of two parallel pipes with  $Q_d = 265/2 = 132.5$  m<sup>3</sup> s<sup>-1</sup> each.

**Table 4**  
Darcy-Weisbach Friction Factor as a Function of the Parts of the Cross-Sectional Perimeter With Mussel Attachment and the  $k_s$  Value of the Mussel Patches

	Typical trapezoidal cross-section $R_h \approx 5.0$ m			Typical U-shaped cross-section $R_h \approx 2.6$ m			Typical circular cross-section $R_h \approx 0.9$ m	
	(i)	(i)-(ii)	(i)-(iii)	(i)	(i)-(ii)	(i)-(iii)	(i)	(i)-(ii)
$k_s = 0.91$ mm		0.0092			0.0095		0.0127	
$k_s = 5$ mm	0.0096 (+4%)	0.0098 (+7%)	0.0100 (+9%)	0.0098 (+3%)	0.0113 (+19%)	0.0119 (+25%)	0.0133 (+5%)	0.0174 (+37%)
$k_s = 17$ mm	0.0099 (+8%)	0.0114 (+24%)	0.0115 (+25%)	0.0103 (+8%)	0.0119 (+25%)	0.0135 (+42%)	0.0168 (+32%)	0.0220 (+73%)
$k_s = 27$ mm	0.0104 (+13%)	0.0117 (+27%)	0.0119 (+29%)	0.0109 (+14%)	0.0132 (+39%)	0.0146 (+53%)	0.0180 (+42%)	0.0243 (+91%)

iii. definition of the patchiness of the mussel biofouling and attribution of the appropriate  $k_s$  value in every grid cell

The part of the wall where mussels preferentially attach was divided into zones, as illustrated in Figures 1b–1d. First, the flow field was simulated without mussels, then with mussels only attached at the preferential wall zone, indicated by i. Subsequently, the mussel-attached zones of the wall were gradually enlarged: first i–ii, then i–ii–iii.

In order to quantify the relevance of mussel biofouling on the energy losses in the application example of the G-WTP, a range of combinations of two parameters was investigated: the first parameter is the part of the cross-sectional perimeter with mussel attachment and the second parameter is the attachment density  $N$  in the mussel-attached parts. For the part of the wall with mussel attachment, the same stages in the colonization succession (Figures 1b–1d) were considered. For attachment density  $N$ , four different configurations were investigated: no or very weak mussel attachment as a reference, low, medium and high attachment densities. The corresponding values of  $N$  are provided in Table 1. They are representative of different reaches of the G-WTP.

iv. estimation of the Darcy-Weisbach friction coefficient  $f$  from the numerical data according to Equation 6 and (v) analysis of the results.

The Darcy-Weisbach friction coefficients estimated from the 3-D numerical simulation are summarized in Table 4 as a function of the parts of the cross-sectional perimeter with mussel attachment and the  $k_s$  value of the mussel patches. Mussel biofouling causes important additional energy losses, as represented by the increase in the Darcy-Weisbach friction factor, even for the relatively small golden mussels in a large hydraulic structure like the G-WTP. In the initial stages of biofouling, when mussels only attach at low attachment density in the preferential patches (indicated by (i)), the overall increase in energy losses is relatively minor (3%–7%) but already non-negligible. The biofouling-induced additional energy losses are highest in the circular cross-sections and lowest in the trapezoidal cross-section, as expected based on the respective values of the relative roughness  $k_s/R_h$ .

The worst-case scenario consists in the largest extension of mussels (patches (i)–(iii) for the trapezoidal and U-shaped cross-sections and the entire wall for the circular cross-section) with the highest  $k_s$  value ( $k_s = 27$  mm), that is, mussels organized in an irregular matrix with irregularities that act as macro-roughness elements. For this worst-case scenario, additional energy losses amount to 29% in the trapezoidal channel, 53% in the open-channel U-shaped aqueduct, and 91% in the pressure-driven flow in the circular pipe. This level of additional energy losses is obviously unacceptable and would endanger the G-WTP's operation.

Interestingly, mussel patches with the highest  $k_s$  value ( $k_s = 27$  mm) on part of the wall (patches (i)–(ii) for the trapezoidal and U-shaped cross-sections and patch (i) for the circular cross-section) cause similar additional energy losses as mussels with the highest attachment density ( $k_s = 17$  mm) covering the largest extension on the wall (patches (i)–(iii) for the trapezoidal and U-shaped cross-sections and the entire wall for the circular cross-section). For the trapezoidal cross-section, the attachment of mussels in patch (iii) hardly influences the energy losses. This is because flow velocities are low near the corner of the cross-section and this flow area only marginally contributes to energy losses.

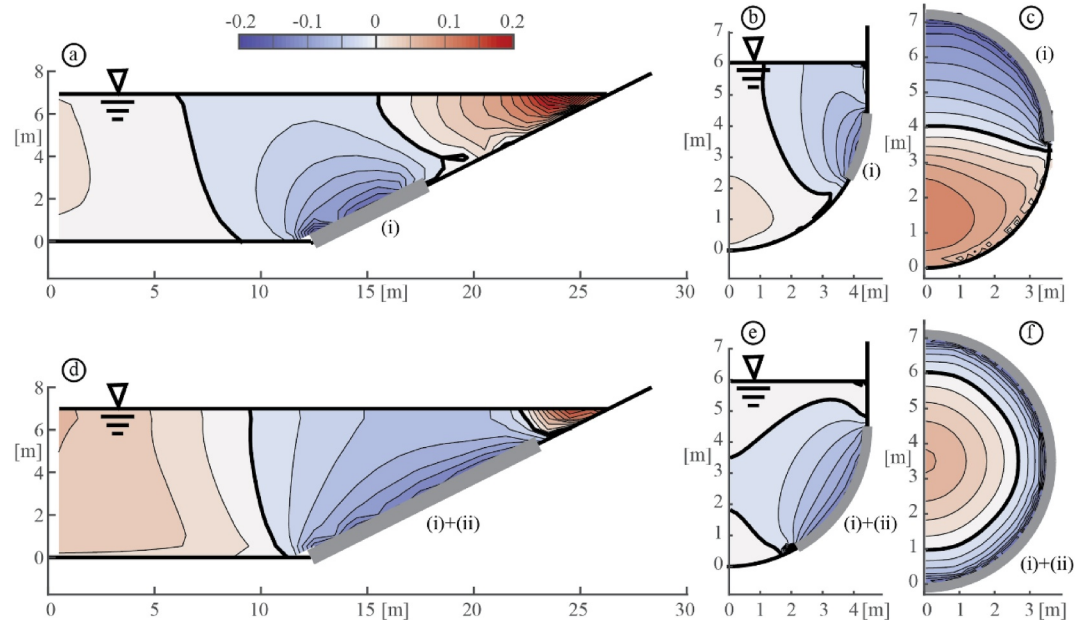


**Figure 6.** Velocity redistribution induced by the mussel biofouling as quantified by the difference between  $u/U$  in configurations with mussel patch (characterized by  $k_s = 27$  mm) and the reference configuration without ( $k_s = 0.91$  mm) in the three typical cross-sectional geometries. (a), (b), (c) Mussel attachment in patch (i); (d), (e), (f) Mussel attachment in patches (i) and (ii). Patches with mussel attachment are indicated by a thick gray line. The thick velocity contour separates regions of increased and decreased  $u/U$ .

The effect of the mussel patches on  $k_s$  values and energy losses is substantiated by the velocity redistributions. Figure 6 shows the difference between the patterns of  $u/U$  with patches of mussel biofouling characterized by  $k_s = 27$  mm and the reference configuration without ( $k_s = 0.91$  mm). An increase of the roughness from  $k_s = 0.91$  mm to  $k_s = 27$  mm causes an important velocity redistribution, even in the large cross-sections of the G-WTP with a relatively low value of  $k_s/R_h = 0.00018$  (Table 4). As expected, the velocity decreases in the vicinity of the roughened mussel patches. Due to mass conservation, this is accompanied by a velocity increase in the central part of the cross-section. For the open-channel flow configurations, a roughening at the wall causes an increase in water surface elevation and a decrease in cross-sectional averaged velocity. This causes a slight bias toward negative values in Figures 6a, 6b, 6d, and 6e. Biofouling at the preferential patch (i) causes a velocity reduction in a substantial part of the cross-section that ranges from the patch at the wall to the free surface in the trapezoidal and U-shaped cross-sections, and that covers approximately half of the cross-section in the circular cross-section. The maximum velocity reduction occurs in the immediate vicinity of the attached mussels and is approximately 15%. At the wall, the zone with reduced velocities extends beyond the mussel patch. A similar velocity redistribution is found when the mussels attach to patches (i) and (ii) at the wall.

From these results, it is clear that mussel biofouling at the walls causes important additional energy losses in most large hydraulic structures, even though the biofouling only causes low values of the relative roughness  $k_s/R_h$ . For the case of the G-WTP, the mussel biofouling endangers its operation and attached mussels should be removed before patches can form that occupy a substantial part of the wall. The results of this application example can be generalized to other water transfer projects confronted with mussel biofouling.

The proposed methodology makes managers and engineers dealing with large hydraulic structures such as water transfer project aware of the importance of heterogeneous patchy roughness distributions and allows estimating the relevance of biofouling-induced additional energy losses. Further numerical and experimental research on heterogeneous roughness distributions would be useful to gain insight in the hydrodynamic processes underlying the additional energy losses.

## 5. Conclusion

Biofouling by mussels significantly affects the roughness of rigid impermeable walls, the flow patterns and the frictional energy losses. Non-dimensional representations of the roughness and the attachment density of patches of mussels are given by  $k_s/L$  and  $N L^2$ , respectively. The dependence of  $k_s/L$  on  $N L^2$  has been investigated in a systematic series of laboratory experiments with mussels sampled in the natural environment for attachment densities in the range  $0.42 < N L^2 < 1.40$  (Figure 4). For values of  $N L^2$  larger than approximately 1.2, the mussels form a continuous regular layer characterized by  $k_s/L \approx 1.5$ . For values in the approximate range  $0.5 < N L^2 < 1.2$ , the mussels rather form a continuous irregular roughness layer with increased values of  $k_s/L$ . These geometrical irregularities are interpreted as macro-roughness elements, that is, roughness elements with a spatial scale larger than that of an individual mussel. For  $N L^2$  smaller than approximately 0.5, the density of the irregularities is too low to act as macro-roughness elements and the resulting  $k_s/L$  value is smaller than that of a continuous regular layer of mussels,  $k_s/L < 1.5$ . These experimental results suggest that  $k_s/L = 1.5$  is a good approximation for the roughness of a continuous regular layer of mussels, and that  $k_s/L = 2.4$  is a conservative estimation for mussels organized in a continuous irregular layer, with irregularities that act as macro-roughness elements. These results provide an estimate of  $k_s$  for mussel-attached walls that is based on the mussel length  $L$ . Thanks to the representation and analysis in terms of non-dimensional variables, it can reasonably be expected that these values are good approximations for a broad range of mussel species with different sizes but similar shapes.

In the reported laboratory experiments no difference exists between the  $k_s$  values of the investigated alive and dead golden mussels (Figure 5), indicating that the effect of the filtering activity is not significant.

A criterion is proposed for the importance of filtering on  $k_s$  (Equation 5), and a quantitative estimation of the threshold value is proposed based on data from the here reported experiments and data reported in literature in other configurations and/or with other mussel species (Table 3). It is found that laboratory conditions are often close to the threshold value (Table 3), but that mussel filtering is always negligible in large hydraulic structures. Such as the investigated G-WTP.

A methodology has been developed for quantifying in a practically useful 1-D framework the energy losses for walls that are only partially covered with patches of mussels and represent a non-homogeneous roughness distribution. The method consists in extracting a Darcy-Weisbach friction factor from a fully 3-D numerical simulation in a simplified reach with constant geometrical properties. The determined friction factor can subsequently be used for the analysis of long systems, such as water transfer projects.

Biofouling-induced energy losses have thus been quantified for the application example of the G-WTP as a function of the patchiness of the mussel attachment and the attachment density in the mussel-attached patches (Table 4). Even in the initial stages of biofouling, when mussels only attach at low attachment density in the preferential patches the overall increase in energy losses is already around 5%. For the worst-case scenario, consisting in the largest extension of mussels with the highest  $k_s$  value, additional energy losses amount to 29% in the trapezoidal channel, 62% in the open-channel U-shaped aqueduct, and 91% in the pressure-driven flow in the circular pipe. Differences between the three geometric configurations are essentially due to different values of the relative roughness  $k_s/R_h$ .

## Data Availability Statement

The experimental data (including measured velocity, and mussel shell length) and ADV data processing code is available in the Zenodo repository (Zhang, Xu, Huber, et al., 2024), which can be accessed at <https://doi.org/10.5281/zenodo.14233518>. This data and code repository has been permanently archived to ensure compliance with FAIR principles, promoting accessibility and reproducibility.

## References

- Alunno-Bruscia, M., Bourget, E., & Fréchet, M. (2001). Shell allometry and length-mass-density relationship for *Mytilus edulis* in an experimental food-regulated situation. *Mar. Ecol. Prog. Ser.*, 219, 177–188. <https://doi.org/10.3354/meps219177>
- Anderson, W., Barros, J. M., Christensen, K. T., & Awasthi, A. (2015). Numerical and experimental study of mechanisms responsible for turbulent secondary flows in boundary layer flows over spanwise heterogeneous roughness. *Journal of Fluid Mechanics*, 768, 316–347. <https://doi.org/10.1017/jfm.2015.91>
- Antico, F., Ricardo, A. M., & Ferreira, R. M. (2019). The logarithmic law of the wall in flows over mobile lattice-arranged granular beds. *Water*, 11(6), 1166. <https://doi.org/10.3390/w11061166>

## Acknowledgments

The study was financially supported by the National Key Research and Development Program of China (Grant 2021YFC3200905), the National Natural Science Foundation of China (Grant U2243222), the monitoring program from South-to-North Water Diversion Middle Route Project (ZXJ/YW/JF-017) and Shenzhen East River Water Source Project Administration (HS421016), the State Key Laboratory of Hydrosience and Engineering Project (Grant 2023-KY-02). We thank Liu Wei and Zhang Tongyu for their help during the experiment. And we thank Prof. Zhang Cheng for his guidance during the data collection. We specially thank the managers from the East River Water Source Project for supporting the experiments.

- Bergeron, N. E., & Abrahams, A. D. (1992). Estimating shear velocity and roughness length from velocity profiles. *Water Resources Research*, 28(8), 2147–2148. <https://doi.org/10.1029/92WR00704>
- Bertin, S., Groom, J., & Friedrich, H. (2017). Isolating roughness scales of gravel-bed patches. *Water Resources Research*, 53(8), 6841–6856. <https://doi.org/10.1002/2016WR020205>
- Boltovskoy, D. (2015). *Distribution and colonization of Limnoperna fortunei: Special traits of an odd mussel*. In D. Boltovskoy (Ed.) (Vol. 10, p. 302). Springer, Cham. Publishing. <https://doi.org/10.1007/978-3-319-13494-9>
- Cannon, D. J., Kibler, K. M., Taye, J., & Medeiros, S. C. (2023). Characterizing canopy complexity of natural and restored intertidal oyster reefs. *Restoration Ecology*, 31(7), e13973. <https://doi.org/10.1111/rec.13973>
- Canovaro, F., Paris, E., & Solari, L. (2007). Effects of macro-scale bed roughness geometry on flow resistance. *Water Resources Research*, 43(10), W10414. <https://doi.org/10.1029/2006WR005727>
- Cao, X. W., Xu, M. Z., Wang, Z. Y., Wang, X. Z., & Liu, M. (2014). Effect of sediment settling on control *Limnoperna Fortunei* bio-fouling in long distance water transport project. *China Rural Water and Hydropower*, 0, 45–48. (in Chinese).
- Carlot, J., Vousdoukas, M., Rovere, A., Karambas, T., Lenihan, H. S., Kayal, M., et al. (2023). Coral reef structural complexity loss exposes coastlines to waves. *Scientific Reports*, 13(1), 1683. <https://doi.org/10.1038/s41598-023-28945-x>
- Cataldo, D., O'Farrell, I., Paolucci, E., Sylvester, F., & Boltovskoy, D. (2012). Impact of the invasive golden mussel (*Limnoperna fortunei*) on phytoplankton and nutrient cycling. *Aquatic Invasions*, 7(1), 91–100. <https://doi.org/10.3391/ai.2012.7.1.010>
- Chen, X., Hassan, M. A., An, C., & Fu, X. (2020). Rough correlations: Meta-analysis of roughness measures in gravel bed rivers. *Water Resources Research*, 56(8), e2020WR027079. <https://doi.org/10.1029/2020WR027079>
- Cheng, N. S. (2011). Representative roughness height of submerged vegetation. *Water Resources Research*, 47(8), W08517. <https://doi.org/10.1029/2011WR010590>
- Darrigran, G. J. B. I. (2002). Potential impact of filter-feeding invaders on temperate inland freshwater environments. *Biological Invasions*, 4(1/2), 145–156. <https://doi.org/10.1023/A:1020521811416>
- Dittrich, A. (1998). Wechselwirkung morphologie/strömung naturnäher fließgewässer. *Mitteilungen des Institutes für Wasserwirtschaft und Kulturtechnik der Universität Karlsruhe. Heft 198. (in German)*.
- Dunker, W. (1856). Mytilacea nova collectionis Cumingiana. *Proceedings of the Zoological Society of London*, 24, 358–366.
- Feng, D. Q., Fan, J. J., Wang, W. J., Xia, C. X., & Li, A. (2024). New formula of vegetation roughness height and Darcy–Weisbach friction factor in channel flow. *Journal of Hydrology*, 636, 131278. <https://doi.org/10.1016/j.jhydrol.2024.131278>
- Ferreira, R. M. (2015). The von Kármán constant for flows over rough mobile beds. Lessons learned from dimensional analysis and similarity. *Advances in Water Resources*, 81, 19–32. <https://doi.org/10.1016/j.advwatres.2014.10.004>
- Ferreira, R. M., Franca, M. J., Leal, J. G., & Cardoso, A. H. (2012). Flow over rough mobile beds: Friction factor and vertical distribution of the longitudinal mean velocity. *Water Resources Research*, 48(5). <https://doi.org/10.1029/2011WR011126>
- Frau, D., Molina, F. R., Devercelli, M., & de Paggi, S. J. (2013). The effect of an invading filter-feeding bivalve on a phytoplankton assemblage from the parana system: A mesocosm experiment. *Marine and Freshwater Behaviour and Physiology*, 45(5), 303–316. <https://doi.org/10.1080/10236244.2012.735419>
- Gaudio, R., Miglio, A., & Dey, S. (2010). Non-universality of von Kármán's  $\kappa$  in fluvial streams. *Journal of Hydraulic Research*, 48(5), 658–663. <https://doi.org/10.1080/00221686.2010.507338>
- Goring, D. G., & Nikora, V. I. (2002). Despiking acoustic Doppler velocimeter data. *Journal of Hydraulic Engineering*, 128(1), 117–126. [https://doi.org/10.1061/\(ASCE\)0733-9429\(2002\)128:1\(117\)](https://doi.org/10.1061/(ASCE)0733-9429(2002)128:1(117))
- Guta, H., Hurther, D., & Chauchat, J. (2022). Bedload and concentration effects on turbulent suspension properties in heavy particle sheet-flows. *Journal of Hydraulic Engineering*, 148(7). [https://doi.org/10.1061/\(ASCE\)HY.1943-7900.0001988](https://doi.org/10.1061/(ASCE)HY.1943-7900.0001988)
- Guta, H., Hurther, D., & Chauchat, J. (2024). Turbulent kinetic energy budget of sediment-laden open-channel flows: Bedload-induced wall-roughness similarity. *Journal of Fluid Mechanics*, 987(A25), A25. <https://doi.org/10.1017/jfm.2024.354>
- Hinze, J. O. (1975). *Turbulence* (2nd ed.). McGraw-Hill.
- Hurther, D., & Lemmin, U. (1998). A constant beamwidth transducer for three-dimensional Doppler profile measurements in open channel flow. *Measurement Science and Technology*, 9(10), 1706–1714. <https://doi.org/10.1088/0957-0233/9/10/010>
- Ito, K., & Takimoto, G. (2013). Prediction of expansion of golden mussel, *Limnoperna fortunei*, in Lake Kasumigaura using a meta-population model. *Japanese Journal of Benthology*, 63, 30–34. [In Japanese].
- Kempf, G. (1937). On the effect of roughness on the resistance of ships. *Trans INA*, 79, 109–119.
- Krzywinski, M., & Altman, N. (2014). Visualizing samples with box plots: Use box plots to illustrate the spread and differences of samples. *Nature Methods*, 11, 119–121.
- Lazzarin, T., Constantinescu, G., Di Micco, L., Wu, H., Lavignani, F., Lo Brutto, M., et al. (2023). Influence of bed roughness on flow and turbulence structure around a partially-buried, isolated freshwater mussel. *Water Resources Research*, 59(4), e2022WR034151. <https://doi.org/10.1029/2022WR034151>
- Li, D. M. (2009). Study on the effect of golden mussel on the water conveyance capacity of water conveyance structures. *Water & Wastewater Engineering*, 45(S1), 94–96. [in Chinese].
- Liu, W., Xu, M. Z., Zhang, J. H., & Zhang, T. Y. (2020). Survival and attachment of biofouling freshwater mussel (*Limnoperna fortunei*) to environmental conditions: Potential implications in its invasion, infection and biofouling control. *Limnology*, 21(2), 245–255. <https://doi.org/10.1007/s10201-020-00607-1>
- Moody, L. F. (1944). Friction factors for pipe flow. *Transactions of the ASME*, 66(8), 671–678. <https://doi.org/10.1115/1.4018140>
- Morton, B. (1973). Some aspects of the biology and functional morphology of the organs of feeding and digestion of *Limnoperna fortunei* (Dunker) (Bivalvia: Mytilacea). *Malacologia*, 12, 265–281.
- Nezu, I., & Nakagawa, H. (1993). *Turbulence in open-channel flows*. Balkema.
- Nikuradse, J. (1932). Gesetzmäßigkeiten der Turbulenten Strömung in Glatten Rohren (Laws of turbulent flow in smooth pipes). *VDI – Forschungsheft 356, Ausgabe B*, 3, 1–36. (Translation: NASA TT F-10, 359, October 1966).
- Nikuradse, J. (1933). Strömungsgesetze in rauhen Rohren (Laws of flow in rough pipes). *VDI – Forschungsheft 361, Ausgabe B 4*. (Translation: NACA TM 1292, November 1950).
- Pestana, D., Ostrensky, A., Boeger, W. A. P., & Pie, M. R. (2009). The effect of temperature and body size on filtration rates of *limnoperna fortunei* (Bivalvia, Mytilidae) under laboratory conditions. *Brazilian Archives of Biology and Technology*, 52(1), 135–144. <https://doi.org/10.1590/S1516-89132009000100018>
- Prandtl, L. (1956). *Führer durch die Strömungslehre* (4th ed., p. 407). Vieweg and Sohn. (in German).
- Qin, X. C. (2021). Study on the value range of roughness of water conveyance tunnel in the Pearl River Delta water resources allocation project. *Guangdong Water Resources and Hydropower*, 04, 31–34. [in Chinese].

- Ricciardi, A. (1998). Global range expansion of the Asian mussel *Limnoperna fortunei* (Mytilidae): Another fouling threat to freshwater systems. *Biofouling*, 13(2), 97–106. <https://doi.org/10.1080/08927019809378374>
- Rouse, H. (1943). Evaluation of boundary roughness. In *Proceedings second hydraulics conference*. University of Iowa.
- Rouse, H. (1950). *Engineering hydraulics* (p. 1039). Wiley and Son.
- Rückert, G., Mônica de Cassia, S. C., & Maria Edith, R. (2004). Alimentação de *Limnoperna fortunei* (Dunker 1857): Taxas de filtração com ênfase ao uso de Cyanobacteria. *Acta Scientiarum. Biological Sciences*, 26(4), 421–429. <https://doi.org/10.4025/actasciobiolsci.v26i4.1523>
- Sandbach, S. D., Lane, S. N., Hardy, R. J., Amsler, M. L., Ashworth, P. J., Best, J. L., et al. (2012). Application of a roughness-length representation to parameterize energy loss in 3-D numerical simulations of large rivers. *Water Resources Research*, 48(12), W12501. <https://doi.org/10.1029/2011WR011284>
- Sansom, B. J., Atkinson, J. F., & Bennett, S. J. (2018). Modulation of near-bed hydrodynamics by freshwater mussels in an experimental channel. *Hydrobiologia*, 810(1), 449–463. <https://doi.org/10.1007/s10750-017-3172-9>
- Sansom, B. J., Bennett, S. J., & Atkinson, J. F. (2022). Freshwater mussel burrow position and its relation to streambed roughness. *Freshwater Science*, 41(2), 315–326. <https://doi.org/10.1086/719993>
- Sansom, B. J., Bennett, S. J., Atkinson, J. F., & Vaughn, C. C. (2020). Emergent hydrodynamics and skimming flow over mussel covered beds in rivers. *Water Resources Research*, 56(8), e2019WR026252. <https://doi.org/10.1029/2019WR026252>
- Schlichting, H., & Gersten, K. (2017). *Boundary-layer theory* (9th ed., p. 805). Springer.
- Schultz, M. P. (2007). Effects of coating roughness and biofouling on ship resistance and powering. *Biofouling*, 23(5), 331–341. <https://doi.org/10.1080/08927010701461974>
- Styles, R. (2015). Flow and turbulence over an oyster reef. *Journal of Coastal Research*, 31(4), 978–985. <https://doi.org/10.2112/JCOASTRES-D-14-00115.1>
- Sylvester, F., Dorado, J., Boltovskoy, D., Juarez, A., & Cataldo, D. (2005). Filtration rates of the invasive pest bivalve *Limnoperna fortunei* as a function of size and temperature. *Hydrobiologia*, 534(1–3), 71–80. <https://doi.org/10.1007/s10750-004-1322-3>
- Tang, B., & Riisgard, H. U. (2018). Relationship between oxygen concentration, respiration and filtration rate in blue mussel *Mytilus edulis*. *Journal of Oceanology and Limnology*, 36(2), 395–404. <https://doi.org/10.1007/s00343-018-6244-4>
- Thomas, F. N., & Schloesser, D. W. (2013). *Quagga and zebra mussels: Biology, impacts, and control* (2nd ed.). Taylor and Francis Group.
- Tokumon, R., Cataldo, D., & Boltovskoy, D. (2016). Effects of suspended inorganic matter on filtration and grazing rates of the invasive mussel *Limnoperna fortunei* (Bivalvia: Mytiloidea). *Journal of Molluscan Studies*, 82, 201–204. <https://doi.org/10.1093/mollus/eyv024>
- Van Duren, L. A., Herman, P. M. J., Sandee, A. J. J., & Heip, C. H. R. (2006). Effects of mussel filtering activity on boundary layer structure. *Journal of Sea Research*, 55(1), 3–14. <https://doi.org/10.1016/j.seares.2005.08.001>
- Vermaas, D. A., Uijtewaal, W. S. J., & Hoitink, A. J. F. (2011). Lateral transfer of streamwise momentum caused by a roughness transition across a shallow channel. *Water Resources Research*, 47(2). <https://doi.org/10.1029/2010wr010138>
- Wu, H., Constantinescu, G., & Zeng, J. (2020). Flow and entrainment mechanisms around a freshwater mussel aligned with the incoming flow. *Water Resources Research*, 56(9), e2020WR027983. <https://doi.org/10.1029/2020WR027983>
- Yao, G. Y., Xu, M. Z., & An, X. H. (2017). Concrete deterioration caused by freshwater mussel *Limnoperna fortunei* fouling. *International Biodeterioration & Biodegradation*, 121, 55–65. <https://doi.org/10.1016/j.ibiod.2017.03.011>
- Ye, B. M., Cao, X. W., Xu, M. Z., Wang, Z. Y., & Lin, C. C. (2011). Study of *Limnoperna fortunei* invasion in water transport project. *Water and Wastes Engineering*, 37, 99–102.
- Zhan, A. B., Zhang, L., Xia, Z. Q., Ni, P., Xiong, W., Chen, Y. Y., et al. (2015). Water diversions facilitate spread of non-native species. *Biological Invasions*, 17(11), 3073–3080. <https://doi.org/10.1007/s10530-015-0940-1>
- Zhang, J. H., Xu, M. Z., Huber, B., Grünzner, M., & Blanckaert, K. (2024). Roughness and energy losses induced by mussel growth on the walls of hydraulic structures and application to a water transfer project (v1.0) [Dataset]. *Zenodo*. <https://doi.org/10.5281/zenodo.14233518>
- Zhang, J. H., Xu, M. Z., & Yang, Y. (2024). Assessing the effects of environmental factors on filtration rates of golden mussel (*Limnoperna fortunei*) applying mussel pump model. *Ecological Indicators*, 158, 111544. <https://doi.org/10.1016/j.ecolind.2024.111544>
- Zhao, N., Xu, M. Z., Blanckaert, K., Qiao, C. H., Zhou, H. M., & Niu, X. L. (2019). Study of factors influencing the invasion of Golden Mussels (*Limnoperna fortunei*) in water transfer projects. *Aquat. Ecosyst. Health*, 22(4), 385–395. <https://doi.org/10.1080/14634988.2019.1698860>